Holzforschung, Vol. 61, pp. 367–374, 2007 • Copyright © by Walter de Gruyter • Berlin • New York. DOI 10.1515/HF.2007.056

Experimental and numerical investigation of wood fracture mechanisms at different humidity levels

Selected article from the 7th WCCM, Los Angeles, USA, July 16–22, 2006

Svetlana Vasic* and Stefanie Stanzl-Tschegg

Institute for Physics and Materials Science, University of Natural Resources and Applied Life Sciences, Vienna, Austria

*Corresponding author.
Institute for Physics and Materials Science, University of Natural Resources and Applied Life Sciences, Peter Jordan Strasse 82, 1190 Vienna, Austria
E-mail: svetlana.vasic@boku.ac.at

Abstract

Differences in fracture patterns and properties at various moisture levels are experimentally and numerically evaluated and discussed. Experiments were performed on spruce, pine, oak and beech. The influence of moisture at 98%, 80%, 65% and 30% RH and the mechanisms involved were investigated for softwoods and hardwoods subjected to opening mode I fracture using *in situ* and *ex situ* real-time environmental scanning electron microscopy (ESEM). The wedge-splitting technique was employed. To quantify the effect of humidity, fracture toughness values were obtained from *ex situ* tests and finite element analysis of the contact problem in wedge-splitting. In addition, lattice fracture model simulations were performed for numerical investigation of the fracture mechanisms. Distinct changes in wood fracture behaviour were observed as a function of moisture content. Fracture toughness was highest at 30% RH for all species except for oak, and showed higher values in the radial-longitudinal than in the tangential-radial direction. In green wood, water droplets moved away from the cell lumens around the crack tip. Drying of wood promotes microcracking and crack bridging as toughening mechanisms. The findings reported may be useful for further research into the interaction between moisture transfer and stress gradients in wood accompanied by moisture-crack phenomena.

Keywords: environmental scanning electron microscopy (ESEM); finite element analysis (FEA); fracture; fracture mechanisms; moisture; numerical modelling; solid wood.

Introduction

Moisture levels are considered as most important environmental effect for wood and its components, as moisture content (MC) influences virtually all the physical and mechanical properties. Adsorbed moisture is known to cause significant dimensional changes, as well as changes in mechanical properties such as the modulus of elasticity, ultimate stress, work of fracture and brittleness.

Tensile and shear strength, as well as fracture toughness in modes I and II, are inversely proportional to MC (Kretschmann and Green 1996). Wang et al. (2003) demonstrated that fracture in wood is related to MC. These authors observed wood at 20°C and at 66%, 82% and 100% RH. MC did not influence the fracture path. With longer moisture absorption times, the time required to reach the maximum load also increased. The maximum fracture toughness was observed at 16.8% MC. King et al. (1999) tested radiata pine as three-point bending single-edge notched (SEN) specimens in mode I, and as compact shear specimens in mode II. They found that mode I fracture toughness was lower for wet wood in all fracture directions than for dry wood. However, in the tangential-radial (TR) direction, fracture toughness was higher for wet wood, whereas in the tangential-longitudinal (TL) direction there was no significant difference between wet and dry wood. Fracture directions (TR and TL) are defined with first letter denoting the plane perpendicular to the crack, and the second the direction of crack growth.

Several studies in the past decade have used environmental scanning electron microscopy (ESEM) of wood microstructural features and fracture. Sippola and Koponen (1999) were the first to apply ESEM to investigate longitudinal tensile fracture in pine. Direct ESEM observations were also successfully performed on saturated wood (Gu et al. 2001). In the ESEM technique, specimens can be hydrated or dehydrated by controlling the temperature of the specimen and the chamber pressure in favour of water condensation or evaporation at different RH values (Wei et al. 2004). The challenges in performing *in situ* ESEM experiments at high MC (so-called low pressure mode) are numerous. Controlled “wet” conditions are usually achieved using a low sample temperature, adequate pressure, a gaseous secondary electron detector (GSED) and a high accelerating voltage. The ESEM technique allows for visualisation of complex wood microstructure under various humidity conditions without applying a conductive coating to the sample.

Green wood is often defined as freshly sawn wood in which the cell walls are completely saturated with water. It also contains water in the cell lumens, known as free water, as opposed to bound water in cell walls. There is no liquid water present in wood below 84% RH (Wadso 1993). In the present study, green woods were conditioned at 98% RH, and then dried to lower levels of 80%, 65% and 30% RH. Fracture processes were investigated by means of *in situ* ESEM experiments, while the fracture properties were obtained from *ex situ* fracture mode I tests. A novel hypothesis was proposed, based on ESEM observations, that stress gradients at the crack tip might have a significant effect on the local moisture distribution, free water flow and vapour diffusion in the vicinity of the crack. The migration of fluid and potential water cluster-

ing and water removal were investigated in the fracture process zone around the crack tip. Wood fracture properties were then characterised and related to different values MC using *ex situ* wedge-splitting tests that showed statistical significance. Quantitative fracture properties were determined to support ESEM observations and strengthen the conclusions. The experimental wedge-splitting set-up with a slightly modified design of the patent of E. Tschegg (1986) and results were also subjected to finite element analysis (FEA) to compute fracture toughness values and to obtain an insight into the local distribution of damage.

Against this background, the phenomena of crack initiation and propagation in wood are not trivial if studied in combination with MC and moisture migration. The present study is only the first step in detecting interrelations in this context by means of *in situ* microscopic observations and quantification of fracture parameters.

Experimental programme

Freshly cut green wood samples of Norway spruce (*Picea abies* [L.] Karst), pine (*Pinus sylvestris*), beech (*Fagus sylvatica* L.) and oak (*Quercus alba*) from Lower Austria were stored in a climate chamber at 98% RH and 20°C. Specimens were cut for monitoring of moisture transfer parameters (weight change versus time) and for mechanical testing. Two different fracture orientations were chosen: radial-longitudinal (RL) and tangential-radial (TR). Each test series consisted of 10 replicates, with eight specimens tested *ex situ* and two tested and examined *in situ* by ESEM.

Micro-wedge-splitting tests of four different species in two fracture directions were performed *ex situ* in a climate box at controlled RH. The set-up in the climate box is shown in Figure 1. Air from a bottle containing salt solution is pumped into the Plexiglass box, which is insulated to prevent humidity loss. A humidity sensor was used to monitor and control RH inside the box. A loading wedge with two rollers moves against the sloped surfaces of the specimen, with geometry adjusted to fit the loading device (Figure 2). The corners were rounded for oak specimens to prevent crack initiation at the locations

Figure 1 Loading wedge-splitting stage inside the climate Plexiglass box.

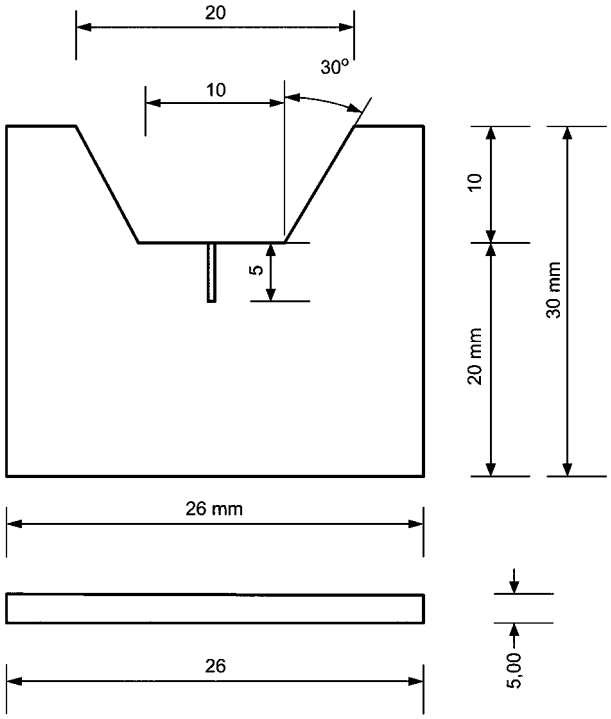

Figure 2 Geometry of the micro-wedge-splitting specimens.

other than the tip of the notch. The rollers reduce the effect of friction in contact. On the opposite side, the loading wedge is connected to a load cell to measure load levels, while one LVDT is attached to a moving block to measure the displacement of the wedge (Stanzl-Tschegg et al. 1995; Frühmann et al. 2003). The displacement rate for both *ex situ* and *in situ* experiments was 6 μm min^{-1}.

Results and discussion

In situ real-time ESEM experiments

In situ ESEM (Philips model XL 30) experiments were performed to investigate changes in the microstructure and fracture pattern in different wood species at four humidity levels. Owing to complexities associated with the ESEM wet mode at high RH, with generally lower image quality than in vacuum, preliminary microstructure observations of the green state were performed using a Peltier cooling stage inside the ESEM at 98% RH, 5°C and 6.5 torr. It is evident from Figure 3a for spruce in the TR direction that some of the lumens are filled with free water, while swelled cell walls indicate complete saturation with bound water. Complete saturation of cell walls and droplets of water in cell lumens were also observed in oak in the TR direction (Figure 3b).

Subsequent to these experiments, *in situ* tests were performed at different RH levels in the ESEM chamber. The cooling temperature was kept constant at 5°C (to avoid freezing), while the pressure was gradually decreased. The operating voltage in wet ESEM mode was 25 kV (which did not cause any beam or sample damage), with a working distance of approximately 10 mm and a spot size between 6 and 7. The loading

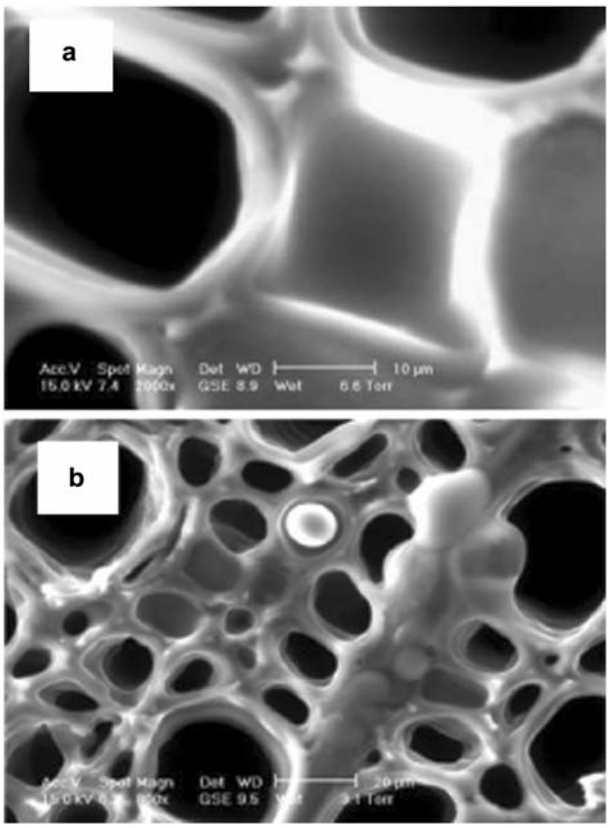

Figure 3 Microstructure in the TR direction in the green state at 98% RH for (a) spruce and (b) oak.

stage was connected to a data-logger and computer, as in the *ex situ* tests, except the LVDT did not fit into the chamber. The loading was stopped intermittently to take pictures once the crack had appeared, and the sample was subsequently reloaded. An example load-displacement *in situ* curve showing that points at which micrographs were taken is presented in Figure 4. The micrographs were always taken in the area of the crack

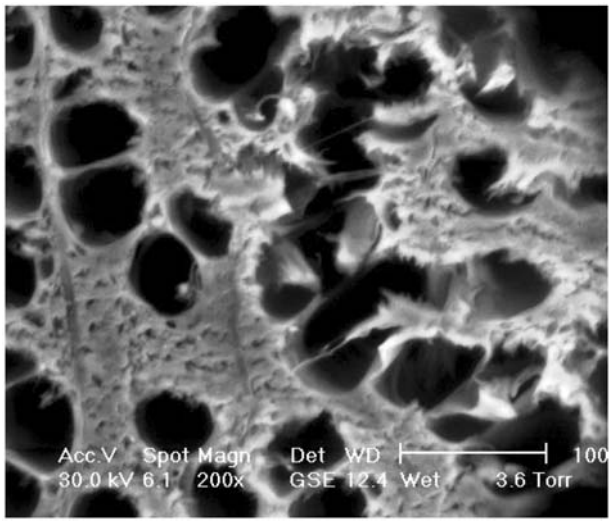

Figure 5 Irregular crack profile in beech in the TR direction at 65% RH with fracture through vessels.

tip and along the fracture path to evidence the crack growth and fracture mechanisms. It was observed that a change of humidity from 98 to 80% RH resulted in evaporation of free water from cell lumens, with the beginning of diffusion of bound water and a small amount of shrinkage.

The discontinuous nature of the crack path, especially in the TR direction and in hardwoods, indicates the extensive formation of undamaged ligaments behind the crack tip and consequent deflection of the crack (Figure 5, beech at 65% RH). The ligaments are several micrometers in size and act to bridge the crack, and have been already identified as the main toughening mechanism in spruce at very low MC in vacuum (Vasic and Smith 2002; Smith and Vasic 2003). At lower humidity of 65% and 30%, the crack path in softwoods appears comparatively free of tortuosity, with smaller bridging ligaments and crack-opening displacements. For green wood with the

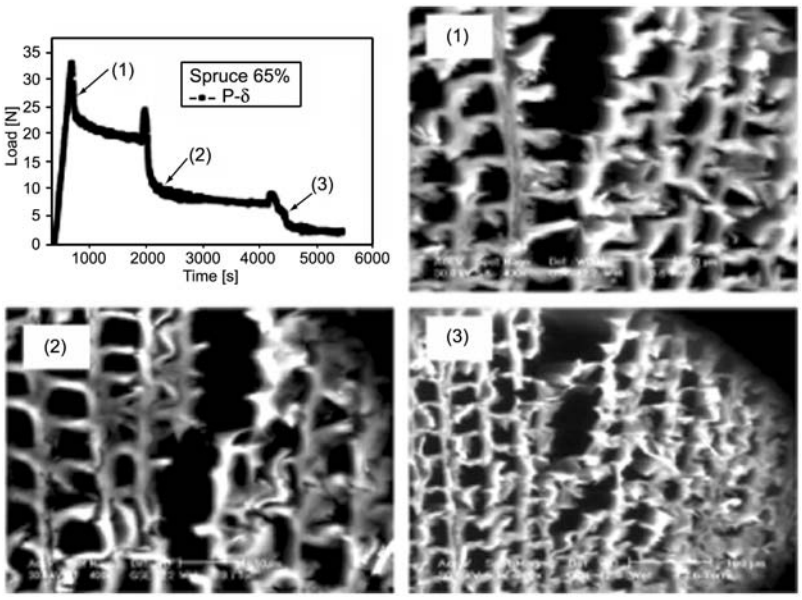

Figure 4 *In-situ P*-δ curve for spruce in the TR direction at 65% RH with representative micrographs in the post-peak regime of crack propagation.

presence of free water, the most important observation is that water droplets from cell lumens move away from the crack tip and the fracture process zone (in the TR direction, a few cells around the crack profile), as no water was observed remaining in the crack tip region. The fluid seemed to be "squeezed out" from the crack tip region prior to extension of the crack. This is in apparent contrast to many similar observations and hypotheses in other materials, with fluid ingress at the crack tip and egress in the crack wake during subcritical cracking. It can be concluded that crack propagation resistance in green wood is not influenced by fluid pressure around the crack tip. These conclusions are important for proper choice of a physically based theoretical model to describe fracture resistance of wood in the drying process.

Ex situ wedge-splitting tests and numerical analysis

Averaged load-displacement curves for all four wood species in the green state are shown in Figure 6a (RL direction) and Figure 6b (TR direction). From the experimental curves, several mechanical parameters could be obtained: the maximal load and corresponding displacement, the initial stiffness and the specific fracture energy. The initial slope corresponds to the linear elastic stiffness of the material at a specific moisture level. The specific fracture energy corresponds to the integrated area under the load-displacement curve divided by the nominal fracture surface area. Due to the nominal stability of the fracture processes recorded, it was possible to calculate the specific fracture energy for all specimens tested.

Figure 6a shows that spruce and pine exhibit very ductile response, while oak was the strongest in the RL direction. The mean maximum load was 3.45-fold greater for oak than for spruce. The specific fracture energy was also highest for oak, and was 2.88-fold greater than for spruce. The initial stiffness of the load-displacement curves was also highest for oak. For the softwoods, namely spruce and pine, differences between the mean values are not significant, while the hardwoods, beech and oak, differ to a greater extent. In the TR direction, the fracture responses were more ductile, with much higher strains at the point of crack initiation and stepwise crack propagation in the post-peak regime. The variability of the load-deformation curves in the two directions demonstrates that differences in the microstructure of various wood species play a significant role in the mechanical fracture responses. Trends for the total fracture energy as a function of moisture level and species (Figure 7a) provide a quantitative measure of such

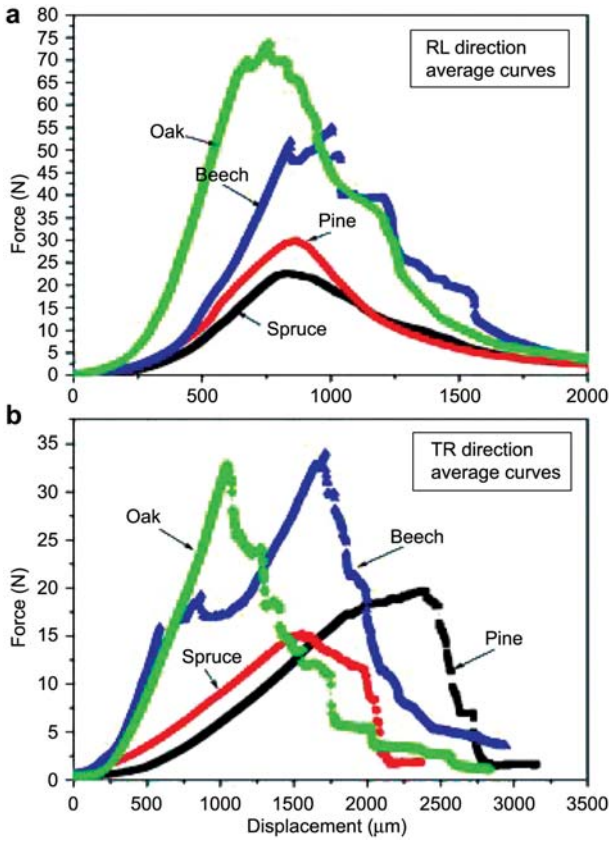

Figure 6 Average load-displacement curves for (a) RL direction and (b) TR direction at 98% RH.

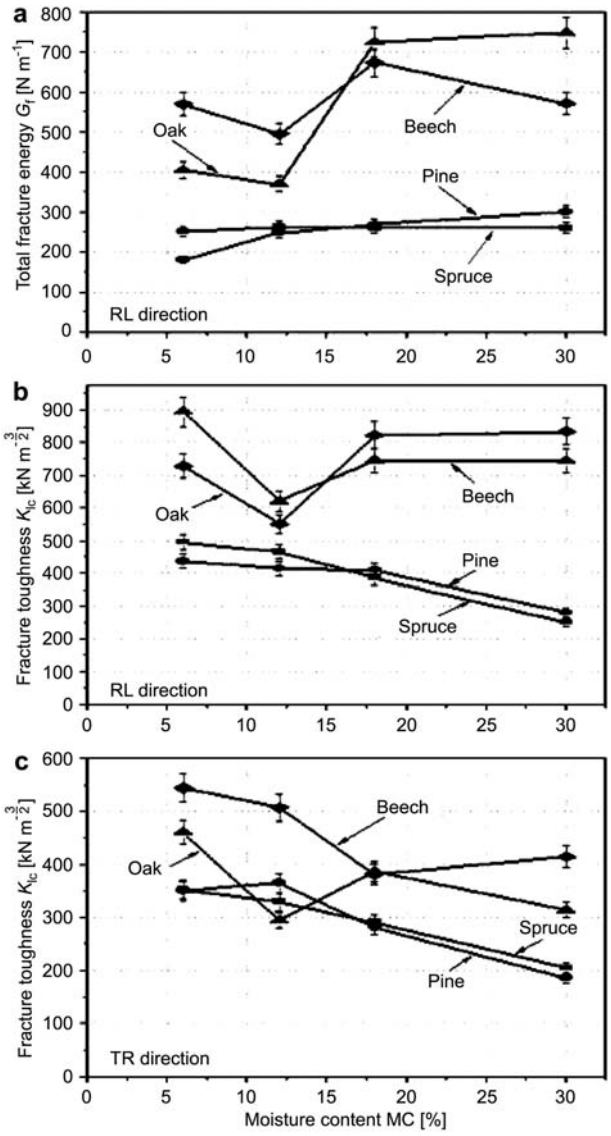

Figure 7 Mean values for different species, with error bars for 95% confidence interval for mean values: a) specific fracture energy RL, b) fracture toughness RL, c) fracture toughness TR.

responses. Oak and pine exhibited an apparent gain in total fracture energy with increasing moisture.

Simultaneously with experimental fracture investigation, numerical analysis of the wedge-splitting test set-up and *ex situ* results was performed using the finite element method and ABAQUS 6.5 commercial software. Numerical simulations are necessary to compute wood fracture toughness, since such specimens are not standard and orthotropic material properties need to be taken into account. Observations of P_{max} were converted into fracture parameters using the finite element method assuming plane strain conditions, with elastic orthotropic parameters taken from Neuhaus (1983) for different MC values for spruce, ranging from 0% to 100%. The following fracture parameters for 12% MC were used: E_L=11,900 MPa, E_R=817.4 MPa, E_T=419.7 MPa, G_{LR}=743.3 MPa, G_{LT}=623.52 MPa, μ_{LR}=0.55, and μ_{LT}=0.41.

Due to symmetry, only half of the model including the contact-crack problem was analysed. Realistic modelling was achieved by application of the wedge force through the roller that first contacts the sample, which yields the deformation and stress distribution at the point of crack initiation. The mesh model is shown in Figure 8, with a magnified area around the initial crack at the notch. The new fracture mechanics module in ABAQUS 6.5 allows for creation of collapsed singular Barsoum elements around the crack tip, with middle nodes moved to a quarter position. Fracture toughness was deduced from values of the *J*-integral, assuming linear elastic fracture behaviour and with orthotropic constants adjusted for the influence of MC. The evaluated and computed mean fracture parameters are listed in Table 1 for green wood (98% RH), in Table 2 for 80% RH, in Table 3 for 65% RH and in Table 4 for 30% RH. Values are given for both RL and TR fracture directions.

Trends for all mean fracture toughness values evaluated for the four species tested and both fracture directions are shown in Figure 7b,c. Each data point on the curves is a mean value for 8–10 replicates. Error bars represent the 95% confidence interval for the mean fracture toughness. Trends in the RL direction seem to be similar for spruce and pine. A constant increase in fracture toughness with decreasing MC is evident, with a maximum at 30% RH (6% MC). The trend for hardwoods (oak and beech) is also similar, although the minimum fracture toughness occurs at 65% RH (12% MC). Differences in wood structural composition correspond to certain degrees of hydration and to different species. This results in variability for fracture toughness values, although the trends can be interpreted in terms of the primary influence of wood microstructure. In the TR

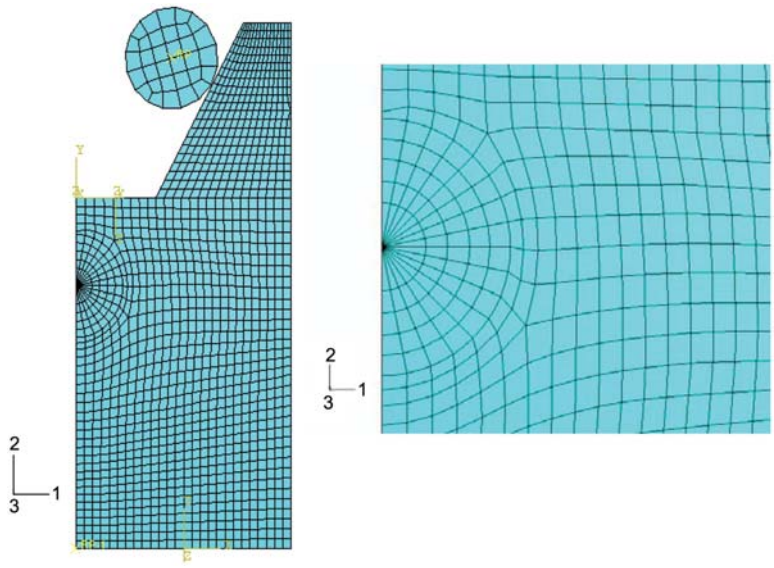

Figure 8 Meshed model of wedge-splitting test set-up with zoomed area around the initial crack.

Table 1 Characteristic parameters for *ex situ* experiments in the RL and TR directions at 98% RH.

	F_{max} [N]	s_{max} [μm]	k_{init} [N mm^{-1}]	G_f [N m^{-1}]	G_{Ic} [N m^{-1}]	K_{Ic} [kN m$^{-3/2}$]
RL						
Spruce	28.75 (11.7%)	962.98 (21.2%)	31.2 (24.9%)	259.43 (25.5%)	124.0 (11.7%)	249.48 (5.6%)
Pine	31.39 (7.11%)	877.65 (4.87%)	35.8 (7.8%)	298.97 (15.4%)	157.96 (7.1%)	280.49 (3.5%)
Beech	85.95 (14.0%)	1094.1 (21.4%)	81.0 (21.2%)	571.87 (16.22%)	427.26 (14%)	743.81 (7.1%)
Oak	99.28 (21.2%)	852.51 (17.2%)	118.1 (23.66%)	747.78 (40.3%)	493.51 (21.2%)	833.44 (10.7%)
TR						
Spruce	23.12 (30.9%)	2339.21 (25.18%)	9.86 (9.08%)	383.99 (36.6%)	328.88 (31%)	204.24 (18%)
Pine	21.17 (27.4%)	1994.85 (26.55%)	10.67 (14.13%)	299.08 (38.5%)	264.8 (38.4%)	185.26 (19.4%)
Beech	51.88 (12.8%)	1195.86 (7.43%)	43.33 (9.2%)	590.83 (24.5%)	543.28 (20%)	413.45 (9.9%)
Oak	41.48 (7.4%)	1261.88 (19.45%)	23.23 (15.06%)	373.35 (12.4%)	313.84 (7.4%)	313.85 (3.7%)

Results are presented as mean (COV).

Table 2 Characteristic parameters for *ex situ* experiments in the RL and TR directions at 80% RH.

	F_{max} [N]	s_{max} [μm]	k_{init} [N mm^{-1}]	G_f [N m^{-1}]	G_{Ic} [N m^{-1}]	K_{Ic} [kN m$^{-3/2}$]
RL						
Spruce	40.68 (29.2%)	0.673 (19.6%)	620.58 (29.4%)	259.59 (21.1%)	209.72 (29.2%)	385.05 (29.2%)
Pine	44.72 (11.4%)	0.842 (35.8%)	610.29 (45.4%)	268.47 (27.9%)	230.52 (11.4%)	409.59 (5.7%)
Beech	115.92 (11.7%)	0.534 (21.0%)	2250.07 (21.5%)	672.68 (19.3%)	519.37 (11.7%)	744.81 (5.8%)
Oak	111.82 (7.5%)	0.656 (19.3%)	1772.94 (23.4%)	723.17 (22.7%)	501.0 (7.5%)	821.95 (3.9%)
TR						
Spruce	29.12 (26.1%)	1.435 (26.9%)	211.06 (26.5%)	471.18 (34.6%)	424.72 (26.1%)	290.26 (12.9%)
Pine	27.32 (24.8%)	1.781 (22.1%)	157.22 (23.3%)	387.4 (25.6%)	378.59 (24.8%)	281.29 (12.5%)
Beech	57.46 (11.5%)	0.991 (25.2%)	606.73 (24.7%)	511.83 (12.6%)	449.18 (11.5%)	380.83 (5.9%)
Oak	73.27 (27.3%)	1.204 (27.0%)	650.71 (36.0%)	621.65 (27.4%)	470.3 (27.3%)	385.99 (15.9%)

Results are presented as mean (COV).

Table 3 Characteristic parameters for *ex situ* experiments in the RL and TR directions at 65% RH.

	F_{max} [N]	s_{max} [μm]	k_{init} [N mm^{-1}]	G_f [N m^{-1}]	G_{Ic} [N m^{-1}]	K_{Ic} [kN m$^{-3/2}$]
RL						
Spruce	68.52 (14.1%)	348 (69.8%)	269.5 (55.2%)	261.49 (13.1%)	241.49 (14.1%)	464.98 (7%)
Pine	54.19 (11.9%)	401 (65.8%)	216.2 (77.9%)	247.78 (26.6%)	190.97 (11.9%)	413.71 (6%)
Beech	141.14 (21.6%)	186 (65.7%)	1325.6 (21.2%)	495.46 (16.22%)	314.65 (21.6%)	620.96 (10.5%)
Oak	110.07 (11.5%)	123 (46.6%)	1187.04 (65.8%)	369.41 (30.2%)	245.4 (11.5%)	550.25 (5.8%)
TR						
Spruce	35.01 (17.8%)	1515 (19%)	24.02 (28.7%)	429.38 (19.3%)	418.62 (17.8%)	328.67 (8.6%)
Pine	64.91 (40.5%)	1726 (37.2%)	37.2 (11.1%)	923.55 (57.7%)	550.22 (40.5%)	364.15 (24.6%)
Beech	84.47 (16%)	612 (12.9%)	141.89 (25.7%)	955.64 (35.1%)	681.9 (16%)	507.22 (7.9%)
Oak	70.38 (15.7%)	648 (89.4%)	226.21 (77.4%)	322.83 (26.8%)	228.7 (15.7%)	293.76 (7.8%)

Results are presented as mean (COV).

direction (direction of drying cracks), this influence is even more pronounced, as no similarity between softwoods and hardwoods is observed. It was noted that values of the *J*-integral were highly dependent on the material stiffness properties, while the fracture toughness values were less sensitive and dependent mainly on the maximum load attained. Wedge displacement as well as time to fracture initiation increased in the RL direction with increasing MC (not shown in the diagrams), as well as with the time fracture initiation. The constant increase in fracture toughness with decreasing MC for spruce in both fracture directions, for example, shows that hydration itself does not involve any toughening effect such as crack blunting, plasticity or viscoplasticity, as in other materials. From Tables 1 and 3 it can be calculated that the increase in spruce stiffness and removal of free water and hydroxyl groups with drying from the green state to 12% MC increased the initiation toughness by ~86% in the RL direction, and by ~61% in the TR direction.

Lattice fracture model simulations

To capture features of damage progression and fracture patterns in wedge-splitting specimens used in the experimental study, a discrete lattice fracture model was applied. Structural elements (finite elements) are arranged in a lattice, and the model is based on morphology (Herrmann and Roux 1990; Landis et al. 2002). The material is represented as an array of nodes connected to a network of discrete beam and spring elements. For orthotropic materials such as wood, a rectangular basic cell is chosen with vertical and diagonal

Table 4 Characteristic parameters for *ex situ* experiments in the RL and TR directions at 30% RH.

	F_{max} [N]	s_{max} [μm]	k_{init} [N mm^{-1}]	G_f [N m^{-1}]	G_{Ic} [N m^{-1}]	K_{Ic} [kN m$^{-3/2}$]
RL						
Spruce	67.23 (18.8%)	0.352 (30.0%)	2122.23 (41.0%)	250.22 (25.4%)	226.25 (18.8%)	494.11 (9.5%)
Pine	58.38 (12.3%)	0.20 (40.8%)	3304.96 (34.1%)	179.8 (22.2%)	151.08 (12.3%)	435.5 (6.0%)
Beech	154.97 (11.2%)	0.28 (29.8%)	6391.37 (52.6%)	569.39 (22.5%)	480.14 (12.0%)	895.33 (5.9%)
Oak	126.4 (17.9%)	0.234 (42.3%)	1263.8 (17.9%)	403.5 (45.3%)	302.5 (17.9%)	727.05 (9.1%)
TR						
Spruce	43.01 (47.6%)	1.822 (14.7%)	253.67 (66.3%)	460.24 (30.6%)	430.08 (47.6%)	352.49 (21.7%)
Pine	51.92 (26.1%)	0.829 (31.0%)	653.81 (23.0%)	410.96 (46.1%)	306.19 (26.1%)	348.8 (12.7%)
Beech	117.89 (12.1%)	0.650 (17.1%)	1838.97 (12.4%)	931.8 (26.6%)	597.15 (12.1%)	544.16 (6.0%)
Oak	75.83 (15.1%)	0.539 (29.6%)	1479.53 (19.8%)	441.52 (18.3%)	427.01 (15.1%)	459.73 (7.5%)

Results are presented as mean (COV).

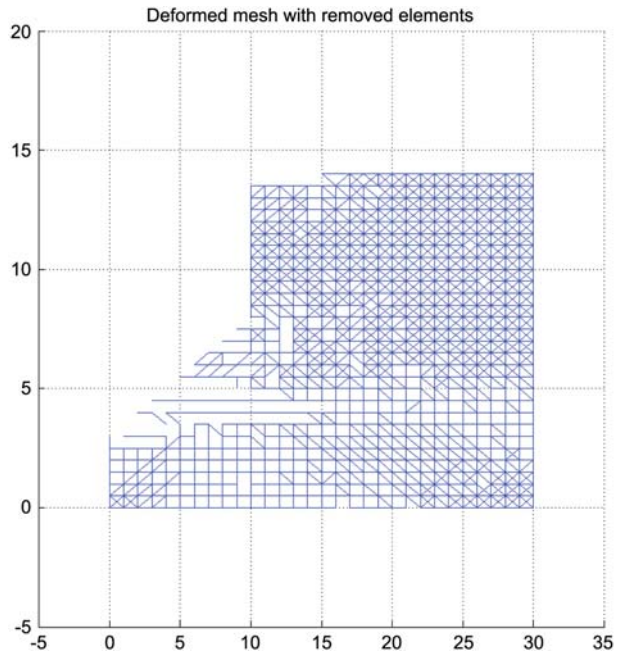

Figure 9 Damage pattern after failure with removed lattice elements.

members (Davids et al. 2003). The model assumes linear elastic brittle failure of elements in tension perpendicular to the grain, which is a realistic approach for behaviour at the local level. This means that once the predefined element strength has been reached, the element is considered broken and is subsequently removed from the lattice geometry.

To account for material heterogeneities, disorder involving statistical variation of element strength and stiffness is added. Specifically, spring constants and strengths are assumed to fit a Gaussian distribution with specified means and standard deviations, resulting in randomness of the local material properties implemented using a Monte Carlo simulation. Element properties were chosen to correspond to the gross stiffness and strength of the material at variable MC. Fracture progression and damage evolution are shown at the end of the simulation at 65% RH in Figure 9. The lattice shows distributed damage in the most stressed regions between the area where concentrated force is applied and the notch plane where the fracture initiates.

Concluding remarks

Load-deformation responses were obtained in *ex situ* experiments, which allowed calculation of the relevant fracture characteristics in two fracture directions: RL and TR. *In situ* real-time ESEM tests were performed, focusing on the fracture mechanisms and qualitative verification of the strong influence of anatomical features on moisture-crack interaction. Experimental findings were interpreted based on the results of finite element analysis.

Several conclusions may be drawn regarding the influence of humidity on fracture behaviour:

1. Moisture influences the fracture properties. Microscopic observations by ESEM provide details of real physical fracture mechanisms.
2. Fracture toughness values K_{Ic} in fracture mode I were highest at 30% RH in both the RL and TR directions. Oak was an exception in the RL direction, for which the maximum was reached in the green state. In spruce, fracture toughness at 65% RH was 86% higher than in the green state in the RL direction and 61% higher in the TR direction.
3. The specific fracture energy G_f was maximum in the green state, except for beech. In general, values were higher in the TR than in the RL direction. Ring-porous hardwood oak showed higher G_f values in the RL direction. The same trend was observed for the energy release rate G_{Ic}.
4. A strong interaction between stress singular crack fields and moisture was observed in the fracture process zone around the crack tip. In green wood, free water was “removed” from most strained wood cells. Water droplets from cell lumens moved away from the crack tip and fracture process zone. Further insight into the physical mechanism of the diffusion of bound water around the crack tip is necessary.
5. Drying of wood was found to promote microcracking and crack bridging behind the crack tip. Crack bridging was induced by the formation of uncracked ligaments in the crack wake. At higher moisture contents, the main characteristics of fracture were tearing of wood cells at higher strain values, and higher crack-opening displacements. The fracture path was dominated by local density variations that depend on the species.
6. Finite element analysis is helpful in interpreting experimental data. Continuum-based analysis was used to compute fracture toughness values and to obtain stress and strain distributions in wedge-splitting specimens. The lattice fracture model demonstrates that the heterogeneous wood microstructure should be taken into account to predict damage patterns.

Acknowledgements

S.V. is grateful for funding obtained from a Marie Curie EU fellowship in Mobility Actions within the Sixth EU Framework Programme.

References

Davids, W.G., Landis, E.N., Vasic, S. (2003) Lattice models for the prediction of load-induced failure and damage in wood. Wood Fiber Sci. 35:120–135.

Gu, H., Zink-Sharp, A., Sell, J. (2001) Hypothesis of the role of cell wall structure in differential transverse shrinkage of wood. Holz Roh Werkst. 59:436–442.

Frühmann, K., Burgert, I., Stanzl-Tschegg, S.E., Tschegg, E.K. (2003) Mode I fracture behaviour on the growth ring scale and cellular level of spruce (*Picea Abies* [L.] Karst.) and beech (*Fagus sylvatica* L.) loaded in the TR crack propagation system. Holzforschung 57:653–660.

Herrmann, H.J., Roux, S. Statistical Models for the Fracture of Disordered Media. North Holland, Amsterdam, 1990.

King, M.J., Sutherland, I.J., Le-Ngoc, L. (1999) Fracture toughness of wet and dry *Pinus radiata*. Holz Roh Werkst. 57:235–240.

Kretschmann, D.E., Green, D.W. (1996) Moisture content-specific gravity relationships for clear southern pine. In: Proceedings of the International Wood Engineering Conference, October 28–31, New Orleans, LA, Vol. 2. Louisiana State University, Baton Rouge. pp. 536–542.

Landis, E.N., Vasic, S., Davids, W.G., Parrod, P. (2002) Coupled experiments and simulations of microstructural damage in wood. Exp. Mech. 42:389–394.

Neuhaus, F.H. (1983) Elastizitätszahlen von Fichtenholz in Abhängigkeit von der Holzfeuchtigkeit. Technisch-wissenschaftliche Mitteilungen Nr. 81-8. Rurh-Universität, Bochum.

Sippola, M., Koponen, S. (1999) Fracture behaviour of clear softwood – Tests and FEM models. In: COST – Action E8: Damage in Wood, Bordeaux. Eds. Morlier, P., Valentin, G. pp. 207–221.

Smith, I., Vasic, S. (2003) Fracture behaviour of softwood. Mech. Mater. 35:803–815.

Stanzl-Tschegg, S.E., Tan, D.M., Tschegg, E.K. (1995) New splitting method for wood fracture characterization. Wood Sci. Technol. 29:31–50.

Tschegg, E.K. (1986) Equipment and appropriate specimen shape for tests to measure fracture values (in German), patent AT-390328.

Vasic, S., Smith, I. (2002) Bridging crack model for fracture of spruce. Eng. Fract. Mech. 69:745–760.

Wadso, L. (1993) Studies of water vapor transport and sorption in wood. Doctoral dissertation. Report TVBM-1013. Building Materials, Lund University, Lund, Sweden.

Wang, L.Y., Lu, Z.Y., Zhao, G.J. (2003) Wood fracture pattern during the water adsorption process. Holzforschung 57: 639–643.

Wei, Q.F., Wang, X.Q., Mather, R.H., Fortheringham, A.F. (2004) New approaches to characterization of textile materials using environmental scanning electron microscope. Fibres Textiles 12:79–83.

Received August 8, 2006. Accepted March 13, 2007.
Published online April 3, 2007.